

EDEM Contact Model: Adhesive Elasto-Plastic Model

Authors:
John P. MORRISSEY
Subhash. C. THAKUR
Jin Y. OOI

School of Engineering,
University of Edinburgh
© *2014*

v1.0f
April 24, 2015

Contents

List of Figures ii

Preface iii

Acknowledgements iv

1 Introduction 1

2 Modelling Approach 2

3 Model Implementation Details 4

3.1 Model Input Parameters 4

4 Contact Model Description 5

4.1 Visco-elasto-plastic adhesive contact model 5

4.1.1 Contact Model Relationships 7

4.2 Normal Force Model 7

4.3 Tangential Force Model 8

4.4 Rolling Friction Model 10

5 References 11

List of Figures

1 SEM images of fine cohesive materials 2
2 Force-separation curves for Agglomerates 3
3 EpAM normal contact force-displacement relationship 5
4 Effect of adhesion exponent and contact plasticity on force-overlap relationship 6

PREFACE

This guide provides the key information regarding an adhesive elasto-plastic contact model for EDEM that has been in development over many years at the University of Edinburgh. The contact model has been implemented as a User Defined Library (UDL) through the API capabilities of EDEM.

This phenomenologically based contact model has evolved over many years of use and development to capture the key bulk behaviour of cohesive powders and granular solids. This guide is written to accompany the contact model and provide the details regarding the motivation and implementation of the contact model. An example problem and description is also provided as an accompanying standalone guide for use with the contact model.

While this version of the contact model has been used and tested extensively, no piece of code is ever completely bug free and, as such, the user should remain vigilant for unexpected outcomes. All efforts have been made to ensure all information is correct at time of writing. The contact model is provided with no explicit guarantee of accuracy or results.

Development never ceases so all further comments, queries or bug reports can be reported to the author or DEM Solutions Ltd.

Dr. John P. Morrissey.
Institute for Infrastructure and Environment,
School of Engineering,
The University of Edinburgh,
Alexander Graham Bell Building, The King's Buildings,
Edinburgh, EH9 3JL
Scotland, U.K.
Email:J.Morrissey@ed.ac.uk

ACKNOWLEDGEMENTS

To acknowledge everyone who contributed to the work over the last few years is not a straight forward task. The significant contributions of Prof. Jian-Fei Chen (now at Queens' University Belfast) and Dr. Jin Sun have been key to the work carried out. The input of other colleagues has also played a role in the continual development of the contact model.

A further acknowledgement and thank you is required for the DEM Solutions team who were always willing to help out and answer the difficult questions when something was not working!

1 INTRODUCTION

The flow behaviour and handling characteristics of cohesive granular solids are strongly dependent on the prior consolidation stress experienced by the solid. As a result, the stress history in the material leading up to a handling scenario needs to be considered when evaluating its handling behaviour. Failure to account for this stress history dependence is ignoring one of the key sources of cohesion for powders and granular solids. For a DEM contact model to successfully capture the real behaviour, it therefore must include contact plasticity and a stress history dependence. along with cohesion.

Many of the other existing contact models such as the JKR, DMT, EDEM linear cohesion model or capillary force models are also elastic models, and as such, may fail to capture the correct stress-history-dependent behaviour. Nevertheless, it has been shown that elastic adhesive models such as the JKR or van der Waals based models can recreate similar initial loose packings and, to a certain extent, capture the initial compression of the material. The initial compression phase can be attributed mainly to particle re-arrangement and occurs at very low stresses (less than approximately 5 kPa).

Much of the handling problems occur in materials where the stress state has been much greater than several kPa and in these situations the elastic adhesive models will not be able to capture the stress-history-dependent behaviour.

An adhesive elasto-plastic contact model [19–21; 25; 27], which will be referred to as the Elasto-plastic Adhesion Model (EpAM) , is implemented in EDEM® through the API functionality of the software. The DEM contact model captures the key characteristic behaviour for agglomerates, where the contact model parameters can easily be calibrated from bulk experiments. The parameters for the contact model are phenomenologically based, with the target of capturing the key bulk characteristics exhibited by the solid. The details for that model are discussed in the following sections.

NOTE 1: COMPILED VERSIONS

The compiled User Defined Library (UDL) is available for both 64-bit Windows and Linux based operating systems.

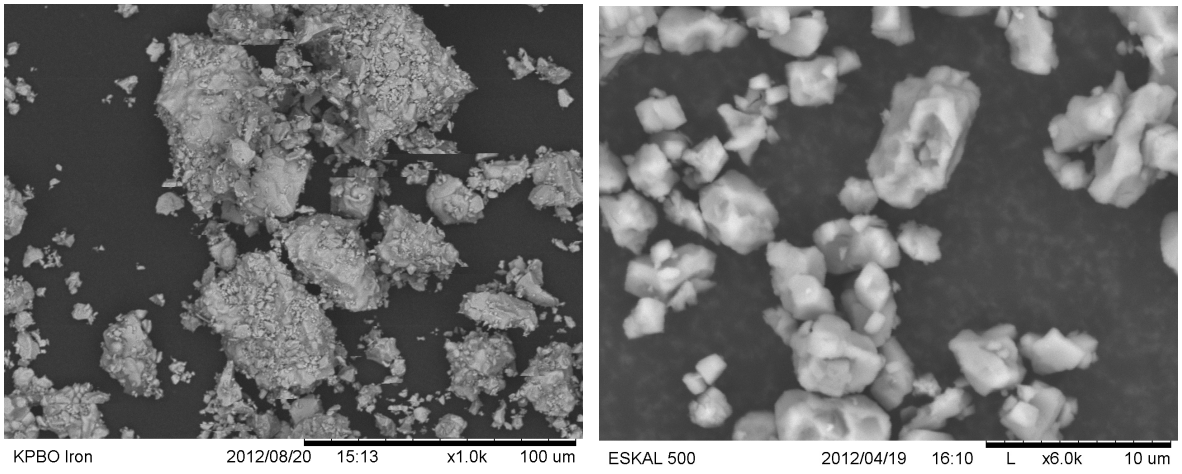
- The Windows version has been compiled in Visual studio 2013 and is compatible with EDEM 2.6. Earlier versions of EDEM may require the Visual Studio 2013 Redistributable package to be installed first.
- The Linux version has been compiled with *gcc* on Scientific Linux 6. This should be compatible with all 64-bit Linux systems and all versions of EDEM.

2 MODELLING APPROACH

Real life particle interactions are incredibly complex and contacts can occur between particles of different sizes and shapes, with individual particles also varying at the contact interface due to the surface roughness of materials. The varying size and shape of particles and surface asperities coupled with various sources of adhesion and factors such as uneven moisture distributions in materials all add to the complexity of granular solids. To apply the model at the single particle level requires the model parameters to be determined at the true particle-particle interaction level. This would require one to consider the enormous complexity of interfacial interaction including the influence of surface topology and chemistry and properties of the interstitial media, etc.

As such, rather than trying to capture the complex micro-mechanical contact behaviour that occurs for the significant number of contacts, a model that will consider the behaviour of bulk solids on a meso-scale rather than micro-scale is envisioned. The methodology employed means that each DEM particle will represent the meso-structure of the bulk material. Interaction properties for this meso-scale interaction can be calibrated from bulk scale experiments rather than measuring microscopic interaction properties, such as friction or adhesion surface energy, for individual microscopic particles.

The reasoning for this approach is simple – firstly, DEM simulations are computationally intensive. To model every individual particle at the real length-scale and include all types of adhesive forces would be prohibitive, meaning that only very small real life systems could be studied within a reasonable time-scale. Also, real particles rarely exist naturally as single particles and are usually found as agglomerates of multiple particles (examples: Figure 1). It is the interaction between these agglomerates that the contact model aims to capture.



(a) Iron Ore Fines - x1K magnification **(b)**Limestone Powder - x6K magnification

FIGURE 1: SEM images of fine cohesive materials - For particles of various sizes

Finally, it should be easier to calibrate on a meso-scale rather than a micro-scale which requires accurate and detailed information on properties such as contact stiffness, pull-off force or moisture distribution. Whilst many studies have been reported on these measurements using microscopic measurement techniques such as AFM, Nano-indentation etc., the measurements tend to be on either highly idealised particles (such as specially manufactured perfect spheres) or suffer from enormous

scatter and uncertainty with regard to the accuracy of the measurement [12; 29].

However, AFM studies can be used to provide valuable information about general behaviour of particles in contact. The contact force-displacement relationship for microscopic particles has been observed by Jones [14] and is depicted in Figure 2. Two particles that are a large distance apart will not experience large attractive forces, however, as the separation distance between the particles reduces, the adhesive force acting between the particle will increase as non-contact forces, such as van der Waals' type force, become more prevalent. A jump-to-contact is observed at very small separation distances. The increased contact areas resulting from plastic deformation leads to an enhanced adhesive strength that needs to be overcome before separation. The studies also reveal the sharp reduction in the adhesion strength of a contact as particles separate, with the possibility of almost 50% of the adhesive force being lost after a very small initial separation.

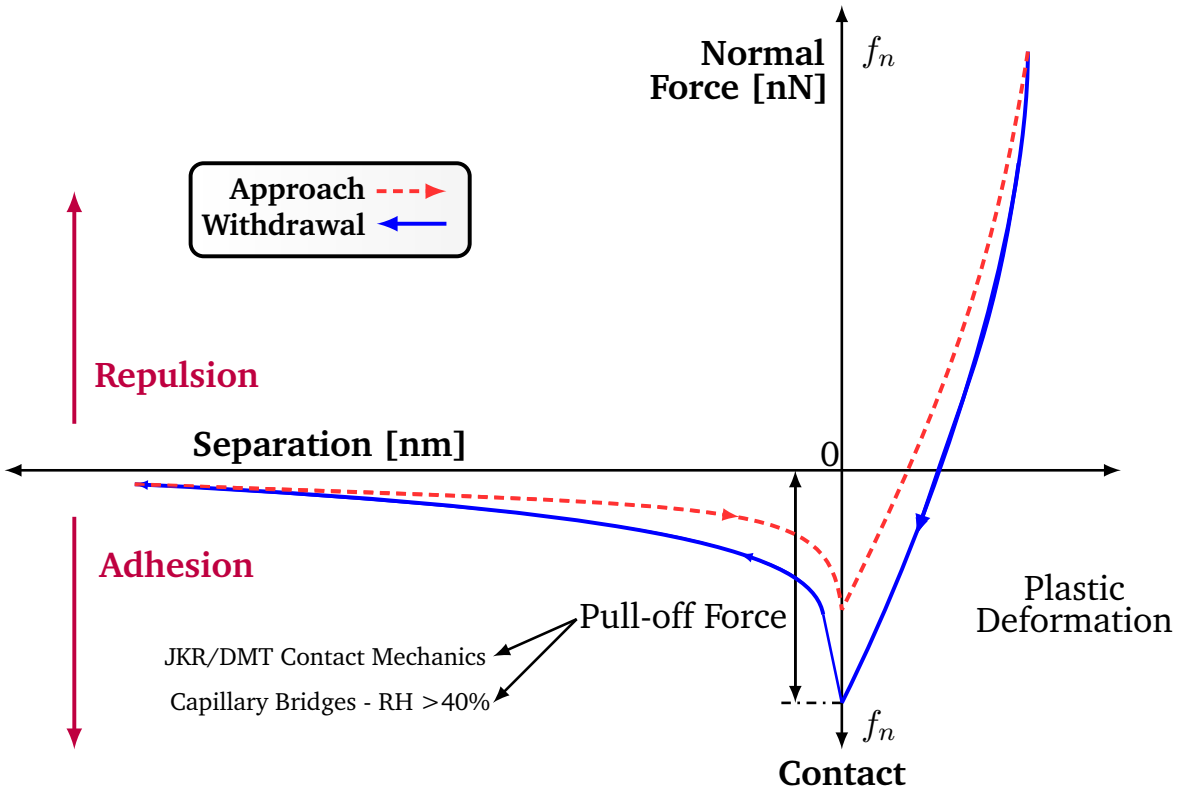


FIGURE 2: Force-separation curves from AFM - Schematic illustration of observed force-separation curves for adhesive particles, adapted from Jones [14]

3 MODEL IMPLEMENTATION DETAILS

EpAM [18; 25] has been implemented in the commercial DEM code EDEM (Versions 2.3+) using the Application Programming Interface (API) feature [7; 9]. Verification of the contact model is presented elsewhere [18].

3.1 MODEL INPUT PARAMETERS

At the initialisation of each simulation, the parameters of the model are loaded into the software from a preference input file (*ECM_Parameters.txt*) which is located in the same folder as the contact model library file.

It contains the following information for the contact model:

- **Constant pull-off force, $\mathbf{f_0}$ (N):** This can be used to incorporate ever presents forces that may occur, such as van der Waals type forces or electrostatic force. The magnitude of this force will not change for the simulation duration.
- **Meso-contact Adhesion Energy, $\Delta\gamma$ ($\mathbf{J/m^2}$):** This is the level of adhesion that is used in the calculation of the load dependent adhesive force in the contact model, f_{min}.
- **Contact Plasticity Ratio, $\lambda_\mathbf{p}$:** Defined as $(1-\frac{k_1}{k_2})$, this is the level of contact plasticity used in the model. This parameter defines the unloading/reloading stiffness k_2 as a constant ratio between the initial stiffness k_1 and the unloading/reloading stiffness k_2. A value of zero represents elastic particle contacts, while a value of one leads to perfectly plastic particle contacts.
- **Power Value for k_1 and k_2 F-D relationship, *n*:** This is used to switch between linear [ECM-L] and non-linear [ECM-NL] force-overlap relationships for the contact model.
- **Power value for adhesion branch, *X*:** This defines the severity of the drop in adhesion force following the peak tensile force being reached. A value of unity gives a linear, more ductile separation curve, whereas a sharp drop in strength is found for values $> X = 2$, which is similar to the separation behaviour depicted in Figure 2.
- **Tangential Stiffness multiplier, $\zeta_\mathbf{tm}$:** This allows the tangential stiffness used in the model to be varied. The tangential stiffness is defined as a ratio of the Virgin Loading Stiffness, k_1 - a multiplier of one gives a tangential stiffness equal in magnitude to the loading stiffness.

These parameters are retained as constants for the duration of the simulation. Parameters can be changed any time the simulation is stopped and restarted, as this will reload the preference file.

NOTE 2: MODEL VERSATILITY

The contact model has an in-built versatility that allows it to be used in several modes:

- If the exponent *n=1* the model will be the well-known linear spring model and if $n = 1.5$ the model will replicate the Hertzian spring model.
- If the level of contact plasticity,$\lambda_\mathbf{p}$, is set to zero then the magnitude of the virgin loading stiffness k_1 and the unloading/reloading stiffness k_2 are equal and the model reverts to being an elastic model.

4 CONTACT MODEL DESCRIPTION

The contact model in its full generic form captures the key elements of the frictional-adhesive contact mechanics in that: f_0 provides the van der Waals type pull-off strength; k_1 and k_2 provide the elastic-plastic contact; the exponent x account for the sudden drop in adhesive strength with increasing separation distance; the exponent n provides non-linearity and the adhesion energy $\Delta\gamma$ in conjunction with the contact plasticity provides the load dependent adhesion limit (see Figure 3). The model is thus expected to be capable of modelling truly micron sized particles to study phenomena such as fine agglomeration, attrition and flow.

4.1 VISCO-ELASTO-PLASTIC ADHESIVE CONTACT MODEL

The DEM contact model [18; 25; 26] is based on the physical phenomena observed in adhesive contact between micron sized particles or small agglomerates [14]. When particles or agglomerates are pressed together, they undergo elastic and plastic deformations. It is assumed that the force required to separate two particles (adhesion) increases with increasing of the plastic contact area. The contact model is non-linear and accounts for both the elastic-plastic contact deformation and the contact-area dependent adhesion. A schematic diagram of particle contact and normal force-overlap ($f_n - \delta$) curve for this model is shown in Figure 3.

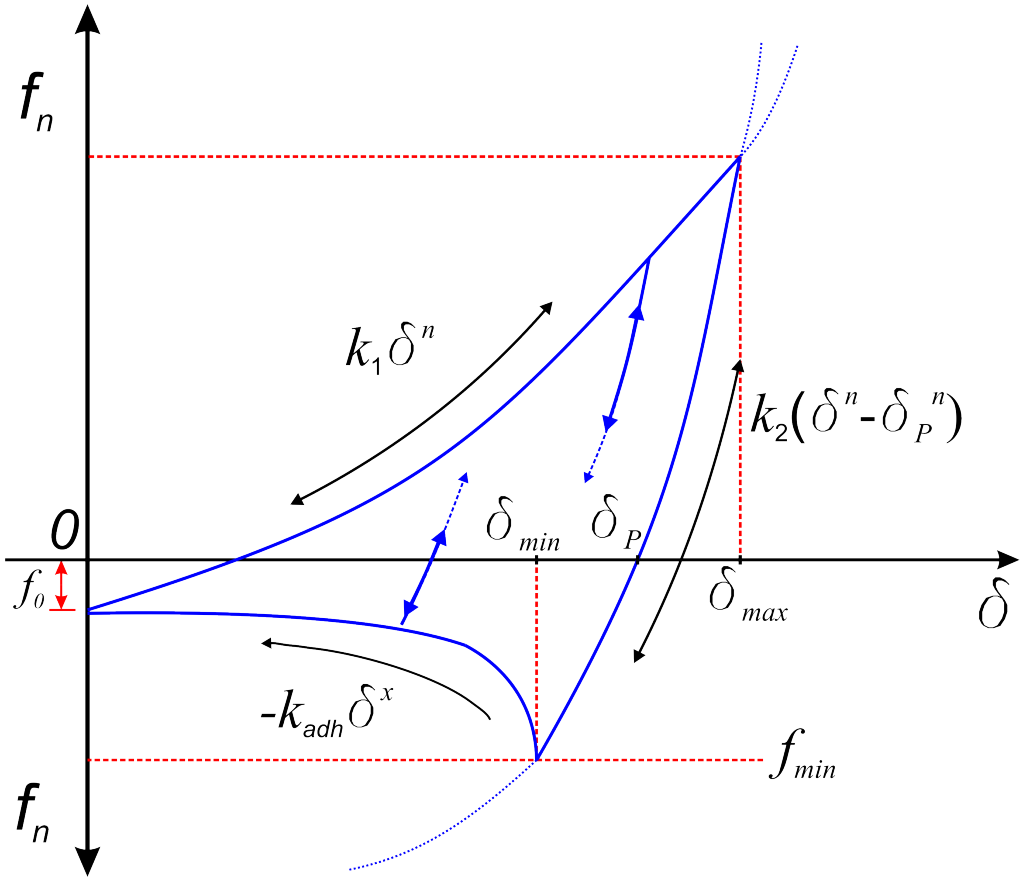
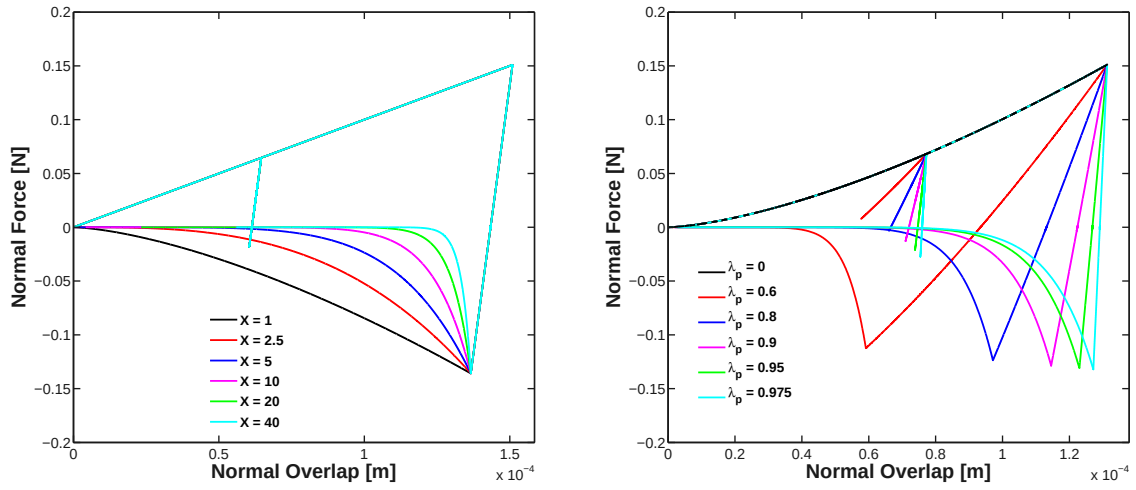


FIGURE 3: EpAM normal contact force-displacement relationship

The loading, unloading/re-loading, and adhesive branches are characterised by seven model parameters: the virgin loading stiffness parameter k_1, the unloading and reloading stiffness parameter k_2,

the Contact Plasticity Ratio, $\lambda_{\mathbf{p}}$, the constant adhesion force f_0, the adhesion energy parameter $\Delta\gamma$, the stiffness exponent *n* and the adhesion exponent χ. The non-linearity of the loading and unloading branches is controlled by the parameter *n* and all become linear when $n = 1$, while the adhesion exponent χ controls the rate at which the adhesion force drops during contact separation - high values represent the sharp drop seen when plastically flattened contacts separate (Figure 2).

Initially, during loading, the contact follows along the virgin loading path k_1. Upon unloading, the contact switches to the unloading/reloading path k_2, reaching zero force at a specific overlap which can be described as the plastic overlap, δ_{p}. If reloading occurs the contact will remain on the k_2 path but switches to the virgin loading path k_1 should the previous historical maximum loading force be exceeded. Unloading beyond the plastic overlap δ_p results in the development of an adhesive force until the maximum adhesive force f_{min} is reached at -$f_0 - k_{adh}\delta_{min}$. Further unloading past this point results in a reduction in both the normal overlap and the attractive force until separation occurs at $\delta = 0$. If reloading of the contact occurs while on the adhesion branch the contact will follow a k_2 path parallel to the initial unloading/reloading path until reaching the virgin loading path k_1. Further loading will then take place on the virgin loading path k_1. The effect of varying Contact plasticity, λ_p, or Adhesion branch exponent, χ, on the force displacement curve for a two particle collision is presented in Figure 4.



(a) Varying Adhesion Exponent, χ **(b)**Varying Contact Plasticity, λ_p

FIGURE 4: Effect of adhesion exponent and contact plasticity on force-overlap relationship - For two particle contact

NOTE 3: INTEGRATION TIMESTEP

The integration timestep, Δt, should be calculated based on the unloading/reloading stiffness k_2. The system should remain stable provided a timestep smaller than $0.17\sqrt{m/k_2}$ is used, where k_2 is $\frac{1}{1-\lambda_p}k_1$.

4.1.1 CONTACT MODEL RELATIONSHIPS

The virgin loading stiffness k_1 is calculated from the specified particle properties in the simulation by Equation (1). The stiffness used is dependent on the particle radius in all cases. The non-linear virgin loading stiffness k_1 is based on Hertz contact Theory while the linear stiffness .

$$k_1 = \begin{cases} 2E^*R^* & \text{if } n = 1 \\ \frac{4}{3}\sqrt{R^*}E^* & \text{if } n > 1 \end{cases} \tag{1}$$

The Contact Plasticity Ratio, λ_p relates the magnitude the the virgin loading stiffness k_1 to the unloading/reloading stiffness k_2 through the following equation:

$$\lambda_p = (1 - \frac{k_1}{k_2}) \tag{2}$$

A value of zero represents elastic particle contacts, while a value of 1 leads to perfectly plastic particle contacts.

Unloading occurs along k_2, reaching zero force at the plastic overlap, δ_{p}, in Equation (3). This maximum plastic overlap is tracked and updated as necessary as the history parameter for the contact model. Historical contact information is only stored while the contact is maintained - "plastic deformation" only exists during a contact.

$$\delta_p = {\lambda_p}^{\frac{1}{n}}\delta \tag{3}$$

The limiting adhesion force for the contact f_{min} is defined by Equation (4). This is the maximum adhesion (pull-off) force that can be sustained by a contact before separation will occur.

$$f_{min} = \pi\Delta\gamma\psi a \tag{4}$$

where $\Delta\gamma$ is the adhesion energy (J/m^2) of the material and ψ is an adhesion constant similar in form to that found in JKR or DMT Theory and *a* is the contact patch radius.

Adopting a value of $3/2$, the minimum adhesive force for the contact is then given by Equation (5), which is similar to that of JKR Theory [13].

$$f_{min} = \frac{3}{2}\pi\Delta\gamma a \tag{5}$$

4.2 NORMAL FORCE MODEL

The total contact normal force $\mathbf{F_N}$ is the sum of the hysteretic spring force, f_{hys}, and the normal damping force, ${f_n}^d$, and is given by

$$\mathbf{F_N} = (f_{hys} + {f_n}^d)\mathbf{u} \tag{6}$$

where $\mathbf{u}$ is the unit normal vector pointing from the contact point to the particle centre. The force-overlap relationship for normal contact, f_{hys}, is then mathematically expressed by

$$f_{hys} = \begin{cases} f_0 + k_1\delta^n & \text{if } k_2\left(\delta^n - {\delta_p}^n\right) \geq k_1\delta^n \\ f_0 + k_2\left(\delta^n - {\delta_p}^n\right) & \text{if } k_1\delta^n > k_2\left(\delta^n - {\delta_p}^n\right) > -k_{adh}\delta^x \\ f_0 - {k_{adh}}^x & \text{if } -k_{adh}\delta^x > k_2\left(\delta^n - {\delta_p}^n\right) \end{cases} \tag{7}$$

The normal damping force, ${f_n}^d$, is given by:

$${f_n}^d = \begin{cases} \beta_L {v_n}^{\overrightarrow{rel}} & \text{if } n = 1 \\ -2\sqrt{\frac{5}{6}}\beta_{NL}\sqrt{K_n m^*}{v_n}^{\overrightarrow{rel}} & \text{if } n > 1 \end{cases} \tag{8}$$

where ${v_n}^{\overrightarrow{rel}}$ is the relative normal velocity between the two particles at their contact and K_n is the Hertzian normal stiffness which is calculated from Equation (9) and depends on the equivalent radius and Young's modulus, as well as the normal overlap δ_{n}.

$$K_n = 2E^*\sqrt{R^*\delta_n} \tag{9}$$

The normal dashpot co-efficient for the linear model (β_L) is given by Equation (10) DEM Solutions Ltd. [5, 6] and for the non-linear model (β_{NL}) by Equation (11)DEM Solutions Ltd. [5, 6].

$$\beta_L = \sqrt{\frac{4m^*k_1}{1 + \left(\frac{\pi}{\ln e}\right)^2}} \tag{10}$$

$$\beta_{NL} = \frac{\ln e}{\sqrt{\ln^2 e + \pi^2}} \tag{11}$$

with the equivalent mass of the particles m* defined as $m_i m_j / m_i + m_j$, and *e* is the coefficient of restitution defined in the simulation.

4.3 TANGENTIAL FORCE MODEL

As both linear and non-linear relationships between load and friction have been found in the literature [2; 3; 11; 15; 22–24], a linear relationship is chosen for two main reasons. Firstly, real materials generally have multi asperity contacts and the literature suggests linear relationship for multi asperity contacts. Secondly, Tomas [28] noted that the normal load response of fine adhesive particles at inter-particle contacts is linear elasto-plastic in most cases with averaged normal macroscopic stresses above 1 kPa and the non-linear behaviour observed in FFM results can be ignored. Therefore, the linear relationship with a constant friction coefficient is deemed suitable.

The limiting tangential friction force is calculated using the Coulombic friction criterion with an addi-

tive term f_0, so that the observed friction is given by

$$f_{ct} = \mu \left| (f_{hys} + k_{adh}\delta^n - f_0) \right| \tag{12}$$

where f_{ct} is the limiting tangential force, f_n is contact normal spring force and μ is the friction coefficient. This is in agreement with experimental results from Skinner and Gane [24], who conducted micro-friction experiments between soft metal stylus and a hard smooth surface of graphite or diamond in a scanning electron microscope and found that the attractive force can be considered as an additive term to the normal force in calculation of limiting friction.

The tangential force is coupled to the normal force satisfying the Coulomb friction criterion such that the tangential force does not exceed the maximum allowed friction value of the shear slider f_{ct}.

$$F_t = \begin{cases} f_t + {f_t}^d & \text{for } f_t \leq \mu_s f_{hys} \\ f_{ct} & \text{for } f_t > \mu_s f_{hys} \end{cases} \tag{13}$$

where μ_s is the coefficient of sliding friction. The force is incremental below the Coulombic Limit f_{ct} that is given by Equation (12), which includes the adhesive contribution [24], and is equal to the limiting friction above the Coulomb Limit.

Therefore, the contact tangential force, F_T, is given by the sum of tangential spring force, f_{ts}, and tangential damping force, f_{td}.

$$F_T = f_{ts} + f_{td} \tag{14}$$

The tangential spring force is expressed in incremental terms

$$f_{ts} = f_{ts(n-1)} + \Delta f_{ts} \tag{15}$$

where $f_{ts(n-1)}$ is the tangential spring force at the previous time step. The increment of the tangential force, Δf_{ts}, is given by

$$\Delta f_{ts} = k_t \delta_t \tag{16}$$

where k_t is the tangential stiffness, and δ_t is the tangential displacement.

The tangential stiffness used for both the linear and non-linear cases is given by Equation (17), where ζ_{tm} is the tangential stiffness multiplier.

$$k_t = \zeta_{tm} \begin{cases} k_1 & \text{if } n = 1 \\ 8G^* \sqrt{R^* \delta_n} & \text{if } n > 1 \end{cases} \tag{17}$$

In the linear case, the tangential stiffness multiplier serves as the link between the normal and tangential stiffness and simply defines the ratio of one to the other - a value of 1 equates the normal and tangential stiffness. The ratio of tangential to normal stiffness for real *elastic* materials lies in the

range of 2/3 to 1, and depends on Poisson's ratio of the material [17] although varying values for this relationship are to be found in the literature [4; 5; 8; 9; 30]. According to Walton [30] both the normal and tangential stiffness are harmonic oscillators and if the model system is to be designed such that the normal spring will be in its equilibrium position at the same time as the tangential spring, then a set ratio of K_t/K_n must be used. For a 2D disc this is given as $K_t = 1/3\ K_n$ and for spheres it is given as $K_t = 2/7\ K_n$.

A value of 2/3 for the tangential stiffness multiplier in the non-linear case returns the relationship suggested by Di Renzo and Di Maio [10], which was found to be one of the best performing tangential models by Kruggel-Emden *et al.* [16] for elastic single particle contacts.

NOTE 4: TANGENTIAL STIFFNESS

The ratio of tangential to normal stiffness varies according to the DEM code and/or contact model being used. Please consult with the relevant literature for exact values of ζ_{tm} used in various codes and contact models.
The values discussed above apply for the case of elastic particle contact and may not necessarily apply in the case of cohesive, plastic particle contacts

The tangential damping force, ${f_t}^d$, is given by:

$$ {f_t}^d = \begin{cases} -\beta_{t,L} {v_t}^{\overrightarrow{rel}} & \text{if } n = 1 \\ -2\sqrt{\frac{5}{6}}\beta_{NL}\sqrt{k_t m^*}\,{v_t}^{\overrightarrow{rel}} & \text{if } n > 1 \end{cases} \tag{18} $$

where ${v_t}^{\overrightarrow{rel}}$ is the relative normal velocity between the two particles at their contact and K_t is the tangential normal stiffness which is calculated from Equation (17) and depends on the equivalent radius and Young's modulus, as well as the normal overlap δ_{n}.

The linear tangential dashpot coefficient $\beta_{t,L}$, is dependent on the tangential stiffness and is given by:

$$ \beta_t = \sqrt{\frac{4m^* k_t}{1 + \left(\frac{\pi}{\ln e}\right)^2}} \tag{19} $$

4.4 ROLLING FRICTION MODEL

While there are many types of rolling friction models available, the type of rolling friction model adopted is a contact independent directional constant torque model, defined as Model Type A by Ai *et al.* [1]. This type of model is used in EDEM in the Hertz-Mindlin model DEM Solutions Ltd. [5, 6]. The total applied torque, τ_i, is given by:

$$ \tau_i = -\mu_r f_{hys} R_i \boldsymbol{\omega_i} \tag{20} $$

where μ_r is the coefficient of rolling friction, R_i is the distance from the contact point to the particle centre of mass and $\boldsymbol{\omega_i}$ is the angular velocity at the contact point.

5 References

[1] Ai, J., Chen, J.F., Rotter, J.M., and Ooi, J.Y. (2011). Assessment of rolling resistance models in discrete element simulations. *Powder Technology*, **206**(3): pp. 269–282. (page 10).

[2] Berman, A., Drummond, C., and Israelachvili, J.N. (1998). Amontons' law at the molecular level. *Tribology letters*, **4**: pp. 95–101. (page 8).

[3] Briscoe, B.J. and Kremnitzer, S.L. (1979). A study of the friction and adhesion of polyethylene-terephthalate monofilaments. *Journal of Physics D: Applied Physics*, **12**(4): pp. 505–516, doi:10.1088/0022-3727/12/4/008. (page 8).

[4] Cundall, P.A. and Strack, O.D.L. (1979). A discrete numerical model for granular assemblies. *Géotechnique*, **29**(1): pp. 47–65. (page 10).

[5] DEM Solutions Ltd. (2010). *EDEM 2.3 User Guide*. DEM Solutions Ltd., Edinburgh, UK, rev. 2c edition, 139 pp. (pages 8, 10).

[6] DEM Solutions Ltd. (2011). *EDEM 2.4 Hertz-Mindlin with JKR cohesion model*. DEM Solutions Ltd., Edinburgh, UK, 6 pp. (pages 8, 10).

[7] DEM Solutions Ltd. (2011). *EDEM 2.4 Programming Guide*. DEM Solutions Ltd., Edinburgh, UK, rev. 1 edition, 49 pp. (page 4).

[8] DEM Solutions Ltd. (2011). *EDEM 2.4 Theory Reference Guide*. DEM Solutions Ltd., Edinburgh, UK, 19 pp. (page 10).

[9] DEM Solutions Ltd. (2011). *EDEM 2.4 User Guide*. DEM Solutions Ltd., Edinburgh, UK, rev. 1 edition, 134 pp. (pages 4, 10).

[10] Di Renzo, A. and Di Maio, F.P. (2005). An improved integral non-linear model for the contact of particles in distinct element simulations. *Chemical Engineering Science*, **60**(5): pp. 1303–1312, doi:10.1016/j.ces.2004.10.004. (page 10).

[11] Ecke, S. and Butt, H.J. (2001). Friction between individual microcontacts. *Journal of Colloid and Interface Science*, **244**(2): pp. 432–435, doi:10.1006/jcis.2001.7959. (page 8).

[12] Heim, L.O., Farshchi, M., and Morgeneyer, M. (2005). Adhesion of carbonyl iron powder particles studied by atomic force microscopy by atomic force microscopy. *Journal of Adhesion Science and Technology*, (February 2013): pp. 37–41. (page 3).

[13] Johnson, K.L., Kendall, K., and Roberts, A.D. (1971). Surface Energy and the Contact of Elastic Solids. *Proceedings of the Royal Society A: Mathematical, Physical and Engineering Sciences*, **324**(1558): pp. 301–313, doi:10.1098/rspa.1971.0141. (page 7).

[14] Jones, R. (2003). From Single Particle AFM Studies of Adhesion and Friction to Bulk Flow: Forging the Links. *Granular Matter*, **4**(4): pp. 191–204, doi:10.1007/s10035-002-0122-6. (pages 3, 5).

[15] Jones, R., Pollock, H.M., Geldart, D., and Verlinden-Luts, A. (2004). Frictional forces between cohesive powder particles studied by AFM. *Ultramicroscopy*, **100**(1-2): pp. 59–78, doi:10.1016/j.ultramic.2004.01.009. (page 8).

[16] Kruggel-Emden, H., Wirtz, S., and Scherer, V. (2008). A study on tangential force laws applicable to the discrete element method (DEM) for materials with viscoelastic or plastic behavior. *Chemical Engineering Science*, **63**(6): pp. 1523–1541, doi:10.1016/j.ces.2007.11.025. (page 10).

[17] Mindlin, R.D. (1949). Compliance of elastic bodies in contact. *Journal of Applied Mechanics*, **16**(259): p. 16. (page 10).

[18] Morrissey, J.P. (2013). *Discrete Element Modelling of Iron Ore Fines to Include the Effects of Moisture and Fines*. Ph.d. thesis, University of Edinburgh. (pages 4, 5).

[19] Morrissey, J.P., Chen, J.F., Ooi, J.Y., Tano, K.T., and Horrigmoe, G. (2012). An Experimental and DEM Study of the Behaviour of Iron Ore Fines. In: *7th International Conference for Conveying and Handling of Particulate Solids - CHoPS 2012*, Friedrichshafen, Germany, pp. 1–10. (page 1).

[20] Morrissey, J.P., Ooi, J.Y., and Chen, J.F. (2013). A DEM study of silo discharge of a cohesive solid. In: *Particle-Based Methods III Fundamentals and Applications - Particles 2013*, (eds.) M. Bischoff, E. Ramm, E. Oñate, R. Owen, and P. Wriggers, International Center for Numerical Methods in Engineering (CIMNE), Stuttgart, Germany, pp. 298–309.

[21] Morrissey, J.P., Ooi, J.Y., Chen, J.F., Tano, K.T., and Horrigmoe, G. (2013). Experimental and discrete element modelling of cohesive iron ore fines. In: *Particle-Based Methods III Fundamentals and Applications - Particles 2013*, (eds.) M. Bischoff, E. Ramm, E. Oñate, R. Owen, and P. Wriggers, International Center for Numerical Methods in Engineering (CIMNE), Stuttgart, Germany, pp. 224–235. (page 1).

[22] Ruths, M., Alcantar, N.A., and Israelachvili, J.N. (2003). Boundary Friction of Aromatic Silane Self-Assembled Monolayers Measured with the Surface Forces Apparatus and Friction Force Microscopy. *The Journal of Physical Chemistry B*, **107**(40): pp. 11149–11157, doi:10.1021/jp0353946. (page 8).

[23] Schwarz, U.D., Zwörner, O., Köster, P., and Wiesendanger, R. (1997). Quantitative analysis of the frictional properties of solid materials at low loads. I. Carbon compounds. *Physical review B*, **56**(11): p. 6987.

[24] Skinner, J. and Gane, N. (1972). Sliding friction under a negative load. *Journal of Physics D: Applied Physics*, **5**: pp. 2087–2095. (pages 8, 9).

[25] Thakur, S., Morrissey, J., Sun, J., Chen, J., and Ooi, J. (2014). Micromechanical analysis of cohesive granular materials using the discrete element method with an adhesive elasto-plastic contact model. *Granular Matter*, **16**(3): pp. 383–400, doi:10.1007/s10035-014-0506-4. (pages 1, 4, 5).

[26] Thakur, S.C. (2014). *Mesoscopic discrete element modelling of cohesive powders for bulk handling applications*. Ph.d. thesis, University of Edinburgh. (page 5).

[27] Thakur, S.C., Ahmadian, H., Sun, J., and Ooi, J.Y. (2013). An experimental and numerical study of packing, compression, and caking behaviour of detergent powders. *Particuology*, (2013), doi:10.1016/j.partic.2013.06.009. (page 1).

[28] Tomas, J. (2007). Adhesion of ultrafine particles - Energy absorption at contact. *Chemical Engineering Science*, **62**(7): pp. 1997–2010, doi:10.1016/j.ces.2006.12.055. (page 8).

[29] Tykhoniuk, R., Tomas, J., Luding, S., Kappl, M., Heim, L.O., and Butt, H.J. (2007). Ultrafine cohesive powders: From interparticle contacts to continuum behaviour. *Chemical Engineering Science*, **62**(11): pp. 2843–2864, doi:10.1016/j.ces.2007.02.027. (page 3).

[30] Walton, O.R. (1994). Force models for particle-dynamics simulations of granular materials. In: *North Amencan Treaty Organization Advanced Study Institute for Mobile Particulate Systems*, December, pp. 1–11, doi:10.1007/978-94-015-8518-7_21. (page 10).